RESEARCH ARTICLE

WILEY

# Dynamic behaviour and seismic response of structures isolated with low shape factor bearings

**Alessandra Orfeo[1]** | **Enrico Tubaldi[1]** | **Alan H. Muhr[2]** | **Daniele Losanno[3]**

[1]Department of Civil and Environmental Engineering, University of Strathclyde, Glasgow, UK

[2]Tun Abdul Razak Research Centre-TARRC, Hertford, UK

[3]Department of Structures for Engineering and Architecture, University of Naples Federico II, Napoli, Italy

**Correspondence**
Alessandra Orfeo, Department of Civil and Environmental Engineering, University of Strathclyde, Glasgow, UK.
Email: alessandra.orfeo@strath.ac.uk

**Abstract**

This study investigates the mechanical behaviour of laminated elastomeric bearings with a low shape factor (LSF) and the dynamic response of structures mounted on them. Axial loads have a significant influence on the mechanical behaviour of the LSF bearings. Most of the existing theories and mechanical models for laminated bearings cannot be employed for LSF bearings because they disregard the important effects of axial shortening and bulging of the rubber layers on the horizontal bearing stiffness.

In this study, a simplified model originally developed for slender rubber blocks is employed for describing the mechanical behaviour of LSF bearings, and validated against the experimental results on low-damping LSF bearings manufactured and tested at Tun Abdul Razak Research Center (TARRC). The proposed model is then used to simulate the seismic response of a structural prototype mounted on the low-damping LSF bearings and tested at University of Naples Federico II on a shaking table under horizontal seismic input. Further analyses are carried out to evaluate how the bearing shape factor affects the dynamic and seismic response of the prototype. The study provides some useful insight into the complex mechanical behaviour of LSF bearings and of structures mounted on them.

**KEYWORDS**
dynamic response, isolation systems, LSF elastomeric bearing, parametric study, simplified numerical modelling

## 1 | INTRODUCTION

Elastomeric laminated bearings are extensively employed to isolate buildings and bridges and protect them from the damaging effect of earthquakes. These devices consist of a number of horizontal rubber layers vulcanized to steel shims.[1,2] This allows to achieve values of the vertical stiffness that are hundreds of times higher than the horizontal stiffness to be achieved, thus ensuring low vertical deflections under permanent loadings together with high flexibility in the horizontal direction. The shape of the rubber layers controls the bearing behaviour in terms of vertical and horizontal stiffness. The

**NOVELTY**

- Evaluation of a mechanical model for elastomeric bearings with low shape factor (LSF).
- Investigation of the dynamic behaviour and seismic response of structure mounted on LSF bearing accounting for the coupling between horizontal and vertical response.
- Review of the existing analytical models for describing the horizontal response of compressed bearings with LSF.
- Simulation of the shaking table tests on a structural prototype mounted on the LSF bearings using simplified numerical modelling approach.
- Numerical investigation of the prototype structure mounted on bearings with different shape factors.

primary shape factor $S$ is a non-dimensional parameter used to describe the bearing geometry, and it is defined as the ratio of the loaded area to the area free to bulge.[3–5] The higher the shape factor, the stiffer the isolator in the vertical direction. Typical values of $S$ are in the range between 15 and 30.[4] With these values, only isolation in the horizontal plane can be achieved. However, in some applications, such as nuclear power plants, isolation in the vertical direction could help to protect sensitive equipment and provide functionality after an earthquake event (see, e.g., ref. [6]). Low-shape factor (LSF) bearings could be used to achieve a three-dimensional seismic isolation (albeit only isotropic in horizontal directions) and/or ensure ground-borne vibration isolation in addition to seismic isolation.[2,7] Moreover, reducing the number of rubber layers and steel plates can yield some cost savings and result in a reduction of the weight of isolators, thus increasing the uptake of seismic isolation in low-income countries. Along the same line, fibre-reinforced elastomeric isolators have been payed increasing interest by several researchers as a lower cost option to traditional systems.[8–10]

LSF bearings have been deployed in many structures and have been the object of numerous investigations over the years. For example, the Pestalozzi school, built in 1969 in Skopje (Macedonia) on unreinforced elastomeric bearings with a shape factor $S = 0.5$, can be thought as a first example of a 3D seismic isolation system.[2] In 1986, Kajima Corporation Technical Research Institute[11] utilized low-shape factor bearings with $S = 2.5$ to support a two-story reinforced concrete building used as acoustic laboratory, demonstrating the effectiveness of the isolation system against both earthquakes and traffic-induced vibrations. Aiken et al.[12] designed and tested LSF bearings to provide three dimensional isolation for a liquid metal reactor building. Zhou et al.[6] and Okamura et al.[13] both considered the application of LSF bearings to 3D isolation of modern nuclear facilities. Cilento et al.[14] also carried out an extensive experimental campaign to demonstrate the effectiveness of isolating a structure with LSF bearing, through the same tests that are considered in this paper. Yabana and Matsuda[15] carried out static, dynamic and failure tests on rubber bearings with thick rubber layers ($S = 4.2$), to evaluate their mechanical characteristics, showing that they are efficient as 3D base isolation devices. It has been highlighted the influence of the decrease of rubber thickness on the vertical stiffness and the good performance of thick rubber layers subjected to very high shear strains (500%). Warn and Wu[16] investigated analytically the concept of LSF as a way to achieve 3D isolation showing that building isolated with LSF bearing could experience minor non-structural damage. Kelly and Lee[17] explored the dynamics of 3D isolation systems and reviewed the existing literature on 3D seismic isolations.

In the last decades, several studies have focused on the evaluation of the mechanical behaviour of rubber isolation bearings, and on the development of simplified mechanical models for describing their response under combined horizontal and vertical loading. Vemuru et al.[18,19] studied both experimentally and numerically the coupled horizontal-vertical behaviour of bearings under quasi-static loading and under dynamic loading. They observed that two behaviours differ considerably from each other. Thus, models describing the variation of horizontal and vertical stiffness with horizontal displacement based on quasi-static tests may not accurately simulate the dynamic response of bearings and structures mounted on them. Few studies have considered specifically LSF bearings and the important effects of the reduction in height and the increase in plan area due to bulging of the rubber layers under compression, which significantly affect the horizontal behaviour. In principle, it could be possible to resort to advanced non-linear 3D finite-element modelling of the bearings[20,21] to capture these effects, as also done by the authors of this study.[22] However, this approach is computationally too expensive and not feasible for the analysis of an entire isolated structure with LSF bearings. For this reason, simplified device models are preferable for evaluating the seismic response of LSF base isolated buildings. In this regard, most of the models available for simulating the horizontal response of laminated bearings under axial loads (mainly due to the gravity loadings acting on the superstructure) (e.g., refs. [23–32]) are based on the theory of Koh and Kelly.[33,34] Thus, they neglect the changes in the geometry of the rubber layers due to the axial loads. A theory based on linear elasticity

and accounting for the nonlinear effect of axial loads on stiffness and on strains and stresses within the rubber was developed by Schapery.[35–37] Bearing properties were derived for different geometries (spherical, flat and cylindrical), loads and deformation modes. Prediction of stiffnesses were also made for LSF values and compared with finite element solutions. Stanton et al.[38] also explored the effect of large deflections on elastomeric bearings taking into account the reduction in height and the increase in plane area due to bulging of the rubber layer under compressive load. More recently, a promising approach for describing the behaviour of LSF bearings was also proposed by Muhr[39] for describing the behaviour of rubber blocks with LSF. Further experimental and numerical studies are required to extend the theory and validate it for the case of laminated bearings.

This paper aims to illustrate and evaluate a mechanical model for LSF bearings and to investigate the dynamic behaviour and seismic response of structures mounted on them by accounting for the coupling between horizontal and vertical response. The first part of the paper describes the results of the experimental campaign carried out at Tun Abdul Razak Research Center (TARRC), consisting of double shear tests on rubber pieces and quasi-static tests on LSF rubber bearings under compression and shear displacements. These results are used to evaluate the suitability of different theories for describing the horizontal response of LSF bearings, including the one of Gent[40] and of Stanton.[38] The results are also used to validate the theory proposed by Muhr[39] for rubber blocks, extended here to the case of LSF bearings.

The second part of the paper focuses on the simulation of the shaking table tests carried out at University of Naples Federico II on a structural prototype mounted on the LSF bearings tested at TARRC.[14] The capabilities of the proposed simplified modelling approach for simulating the behaviour of LSF bearings are investigated by carrying out numerical analyses of the whole isolated system under different earthquake loadings. Further analyses are carried out to compare the performance of the prototype mounted on bearings with different shape factors. The numerical results of the analyses shed light on the possibility of using the simplified model for the preliminary seismic assessment of isolated structures mounted on LSF bearings and on the effect of the bearing shape factor on the seismic performance of structures.

## 2 | MATERIAL AND BEARING TESTS

The first part of this section describes the experimental tests carried out at TARRC to characterise the mechanical behaviour of LSF bearings. These include material tests carried out on small double-shear cylindrical testpieces subjected to sinusoidal shear loading and device tests carried out on LSF bearings subjected to cyclic shear loads under constant compression. Subsequently, the analytical formulation developed by Muhr[39] for LSF rubber blocks is illustrated, together with its extension to the case of laminated bearings, and its capability to describe the bearing behaviour is evaluated based on the comparison with experimental test results. A comparison is also made with the theories of Gent[40] and Stanton et al.,[38] and with some numerical results.[22]

### 2.1 | Experimental tests

Cylindrical in shape with diameter 25 mm, the double-shear testpieces consist of two rubber layers 6 mm thick that have been hot-bonded to metal part. They were made of a lightly filled natural rubber compound and were subjected at TARRC to sinusoidal shear displacement histories with a frequency of 0.5 Hz. It should be noted that the samples were preconditioned (i.e., non virgin). Nevertheless, the stress-softening effects[30,42] are not significant since the compound is a low damping and essentially unfilled natural rubber, and for the same reason the effect of the temperature rise in the rubber upon repeated cycling is negligible. Defining the nominal shear strain $\gamma$ as the ratio between the shear displacement and the rubber height of a single layer, Figure 1(A) shows the results of the tests in terms of variation of the secant shear modulus $G$ with the maximum average shear strain $\gamma_{max}$. The shear modulus $G$ at the maximum shear strain $\gamma_{max}$ is defined as the ratio of the maximum shear stress $\tau_{max}$ and $\gamma_{max}$. The maximum shear stress is defined as the ratio of the maximum shear force to the cross sectional area of the rubber sample. It can be observed that $G$ assumes values in the range between 0.62 and 0.47 MPa, reducing slightly for increasing values of $\gamma_{max}$. Figure 1(B) also shows the variation of the equivalent damping ratio[43] with the strain amplitude. The damping ratio is generally very low, as expected for this type of rubber compound, and increases slightly for increasing $\gamma_{max}$ values.

Figure 2(A) illustrates the tested laminated LSF bearings. These bearings were made from the lightly filled natural rubber compound. They consist of three layers of 19 mm thick rubber, plan size 100 × 100 mm, two internal steel shims (nominal thickness 2 mm), designed to achieve a shape factor $S = 1.32$. The rubber layers were vulcanized and hot-bonded to the steel plates using the Chemosil 211/220 system, as also used for the double shear testpiece of Figure 1. The two
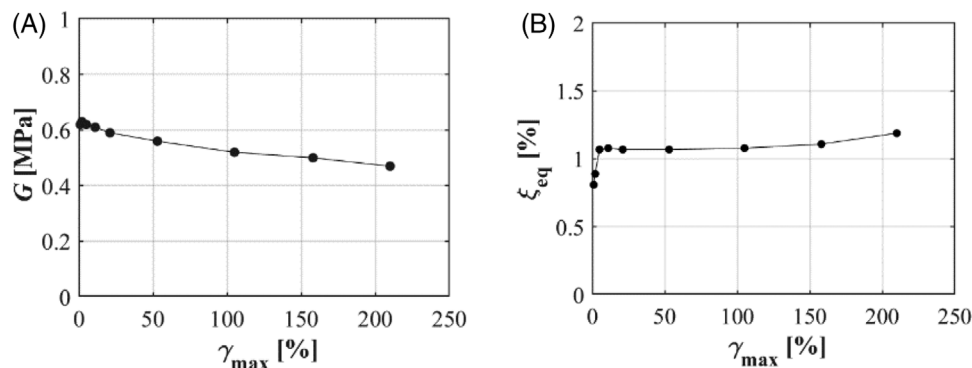
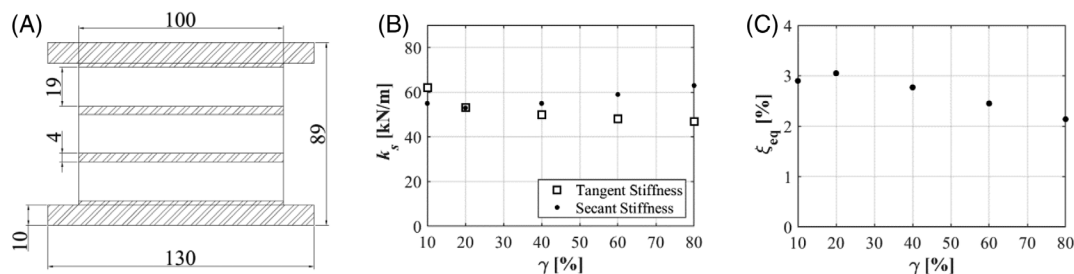**FIGURE 1** Secant shear modulus (A) and equivalent damping ratio (B) versus maximum shear strain.[22]



**FIGURE 2** (A) Bearing geometry, dimensions shown in mm; initial and secant shear stiffness (B) and equivalent damping ratio (C) at different levels of nominal shear strain, under a static displacement equivalent to a load of 19 kN.

internal steel-steel interfaces have been bonded using Loctite 638. Finally steel end plates 130 mm × 100 mm were bonded to the end steel faces using Araldite standard epoxy adhesive. TARRC manufactured four such bearings and performed static compression and dynamic shear loading to a pair of bearing in a double shear configuration. They were subjected to compression displacements using a hydraulic jack, whereas a Dartec uniaxial servohydraulic actuator was used to apply the shear displacements. Two cycles of sinusoidal displacement were imposed at each of a series of increasing shear strain amplitudes.[41,44] It is worth noting that although the bearings were subjected to relatively high horizontal displacement, there were no sign of failures in terms of rubber-to-metal bonding during both these tests and the shaking table tests. Similarly, Yabana et al.[15] observed no bonding failure in their investigation of LSF bearing. However, to reduce the debonding risks, alternative solutions may be employed, for example, using fillets.[45] The hysteresis loops obtained from the sinusoidal tests are used to calculate the secant shear stiffness, defined as follows:

$$k_s = F_{max}/d_{max} \tag{1}$$

where $F_{max}$ is the peak force and $d_{max}$ is the peak displacement.

The horizontal tangent and secant stiffness of the bearing are evaluated considering the second displacement cycle imposed with increasing levels of the nominal shear strain amplitude $\gamma$. Figure 2(B) illustrates the tangent and the secant horizontal stiffness of the bearing under a compressive displacement corresponding to 19 kN. It can be observed that the initial shear stiffness decreases for increasing shear strain amplitudes. On the other hand, the secant shear stiffness first decreases and then increases. This behaviour contradicts the existing literature on elastomeric bearing, which shows a decrease in horizontal stiffness with increasing horizontal displacement.[46,47] This is because the vertical load in the bearings decreases as the lateral displacement increases (see ref. 22). However, the reduction observed in such studies may also be due to the Payne effect, which is the decrease of stiffness for increasing deformation, typical of HDNR compounds.[5,30,42] The Payne effect is not significant in low-damping rubber compounds such as that used for the LSF bearings investigated in this study (see Figure 1B) and thus the observed changes of horizontal stiffness are mainly a geometrical effect. Figure 2(C) illustrates the equivalent damping ratio $\xi_{eq}$ of the bearing at various nominal shear strain amplitudes (i.e., ratio between the bearing horizontal deflection and the total rubber height). It is worth to note that the values of $\xi_{eq}$ range from 2% to 3%, and are substantially greater than the equivalent damping ratio of the rubber compound (around 1%). This phenomenon,

**FIGURE 3** Deformed bearing under a compression load of 19 kN (left) and a combined compression load and shear displacement (right) during the experiment.[44]

observed experimentally by Thomas[48] and numerically by Orfeo,[22] was quantified by Koh and Kelly[34] and Raithel and Serino.[49] They showed, using a viscoelastic analytical model, that the compression load increases the phase difference between the horizontal force and the horizontal displacement, thus increasing the energy dissipation per cycle.

In the tests, a vertical downward displacement was first imposed at the top plate, until a compressive load of 19 kN was achieved, equal to the mean load per bearing under the gravity loads in the shaking table tests. Subsequently, two cycles of sinusoidal displacements were applied while preventing vertical motion and rotation of the top plate. Figure 3 illustrates the deformed bearing during the test under the applied compressive load of 19 kN and the applied load in combination with the maximum applied horizontal displacement.

It is noteworthy that the level of the applied compressive load is 60% higher than the value of the critical bearing load according to the theory of Gent and of Koh and Kelly,[34,40] as also discussed in the subsequent section more in detail. However, no signs of instability were observed in the experiment.

## 2.2 | Review of analytical models of LSF bearings

The behaviour of LSF isolation bearings under shear loading is strongly influenced by the applied compression loads. In particular, compressive loads induce a significant reduction of the horizontal stiffness due to nonlinear geometrical effects (P-delta effects), partly mitigated by the increase of the rubber layer area (due to bulging) and reduction of height. The pressure also increases the damping capabilities under horizontal loading.[34,48,51] An analytical model capable of accurately describing all these effects in bearings for all possible values of shape factors has not been developed, yet. In the following, a brief overview of the theories developed over the years to include axial load effects is provided.

According to the classical theory of rubber blocks, developed under the assumptions of small strains, linear elastic behaviour and incompressibility of the rubber, the vertical load $N$ can be related linearly to the compressive strain $\varepsilon_v$ (i.e., the ratio between the compressive displacement $v_v$ and the undeformed height $h_0$) through the following expression:

$$N = A_0 E_c \varepsilon_v = 3GA_0 \left( f_{c1} + f_{c2} \right) \varepsilon_v \tag{2}$$

where $A_0$ is the initial cross-sectional area of the rubber block, $G$ is the shear modulus and $f_{c1}$ and $f_{c2}$ are numerical factors accounting for the confining effect of the steel plates. Their expressions depend on the rubber section shape and can be found in the original paper of Gent and Meinecke.[56]

The transverse stiffness $k_h$ of an axially loaded shear-flexible beam-column that is fixed against rotation at both ends is.[40,53]

$$k_h = \frac{\alpha \beta N}{2 \tan \left( \frac{\alpha h}{2} \right) - \alpha \beta h} \tag{3}$$

where $h$ is the bearing height between the end plates. The terms $\alpha$ and $\beta$ are defined as follows:

$$\begin{aligned} \alpha^2 &= \frac{N(R+N)}{BR} \\ \beta &= \frac{R}{R+N} \end{aligned} \tag{4}$$

where $B$ and $R$ are the bending and shear stiffnesses for unit length of the rubber column, which are given in different expressions by Gent and Meinecke,[56] and $N$ is the applied vertical load, maintained constant under the horizontal deflection.

The bending and the shear stiffness parameters according to Gent and Meinecke[56] are defined as follows:

$$
\begin{aligned}
B &= f_r E I_0 \\
R &= G A_0
\end{aligned}
\tag{5}
$$

where $f_r$ is a factor that similarly to $f_{c1}$ and $f_{c2}$ accounts for the confinement by the end plates.

The expressions above can be extended to the case of laminated bearings by assuming that the steel layers are rigid, thus increasing the values of $B$ and $R$ according to a factor equal to $h/t_R$, where $t_R$ is the total rubber layer height.[34,57–59]

It is noteworthy that based on the work of Haringx[53] and of Gent,[40] Koh and Kelly[33,34] developed a mechanical model to describe the shear response of elastomeric isolation bearings including the effect of axial loads, and validated it against some experimental results on bearings with values of $S$ in the range 5−10. The dependency of horizontal stiffness on vertical stresses was studied also including large displacements and non-linearity of rubber by other authors.[47,52] These theories assume that the rubber layer shape is fixed and independent of the applied vertical load, which is an accurate assumption only for high shape factors. Thus, they do not account for the reduction of height and bulging (i.e., increase of plan area) of the rubber layers due to compression, which is very significant and cannot be neglected in the case of LSFs.

Stanton et al.[38] derived relations for the compressive, shear and bending stiffnesses of LSF bearings by including the axial shortening and increase in plan area, with the layers' bulging expressed as a function of the Poisson ratio. In the following, reference is made to the "Poisson model", which consists of a homogeneous shear flexible column, made of a linear elastic material and undergoing small deformations. The compressive, shear and bending stiffnesses change with the compressive strain. They are approximated by assuming that the plan dimension of each elastomeric layer increases by a factor $(1 + n^* e_v)$, where $n^* = 0.3$ (rather than 0.5) is a nominal Poisson ratio chosen empirically to account for the non-uniform increase of area along the height due to the effect of the end plates.

The expression of the relationship between the axial force $N$ and the nominal axial deformation $\varepsilon_v$ according to Stanton et al.'s theory[38] is:

$$
N = 3 G A_0 \left( f_{c1} + f_{c2} \right) \frac{(1 + \nu * \varepsilon_v)^3 - 1}{3 \nu * \varepsilon_v} \varepsilon_v
\tag{6}
$$

Stanton et al.[38] provided the following expression of the bending and shear stiffness parameters:

$$
\begin{aligned}
B &= f_r E I_0 (1 + \nu * \varepsilon_v)^4 \\
R &= G A_0 (1 + \nu * \varepsilon_v)^2
\end{aligned}
\tag{7}
$$

These expression of $B$ and $R$ can be used within Equation (3) and assuming $h = h_0$ to evaluate the horizontal stiffness of the compressed bearing.

Muhr[39] adopted the work of Goodchild et al.[51] on the lateral stiffness and damping of stretched rubber beams and developed a theory for the compressive and lateral stiffness of single layer blocks of rubber with bonded endplates under finite axial deformation, accounting for the changes in geometry of the block as functions of the axial shortening and shape factor. The theory of Muhr was developed considering a Mooney–Rivlin strain energy model for the rubber compound, and a simplified deformation field consisting of small shear strains superimposed to finite axial strain.

The expression developed by Muhr[39] for relating the axial compression to the applied compressive load $N$ considering a block made of a Neo-Hookean rubber material is:

$$
N(\lambda) = G A_0 \left[ \left( \lambda - \frac{1}{\lambda^2} \right) + 3 S^2 \left( 1 - \frac{1}{\lambda^2} \right) \right]
\tag{8}
$$

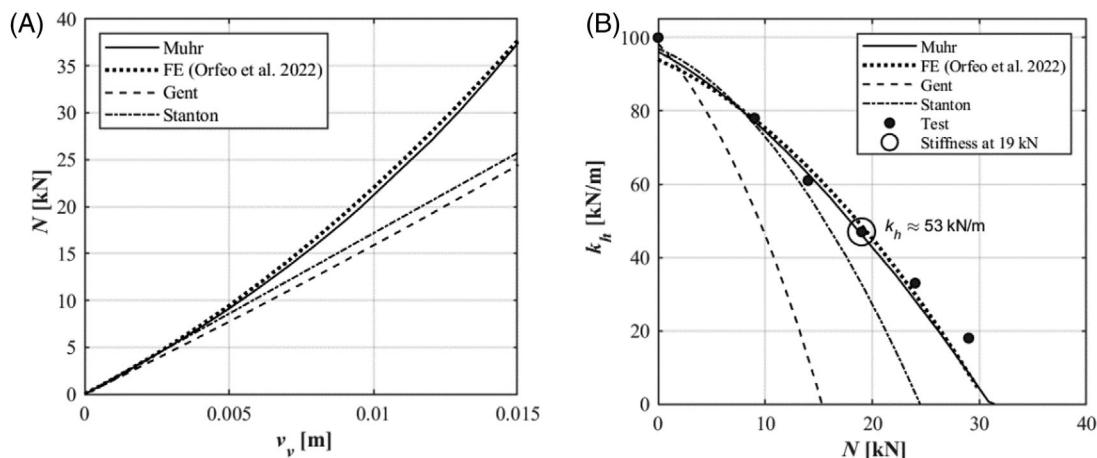where $l = 1-e$ is the axial stretch ratio (<1 in the case of compression).

**FIGURE 4** Comparison between the theories. (A) Compressive load versus vertical displacement (B) Initial shear stiffness versus vertical displacement for the bearing of Figure 2(A). Experimental values taken from ref. 44.

**TABLE 1** Buckling load according to various theories and FE analysis.[22]

| Experimental | Muhr | FE[22] | Gent | Stanton |
| --- | --- | --- | --- | --- |
| 34 kN | 30 kN | 39 kN | 14 kN | 26 kN |

The expressions of $B$ and $R$ according to Muhr are:

$$B = G \left( 2\lambda^2 + \frac{1}{\lambda} \right) \left( 1 + \frac{2S^2}{3} \right) \frac{I_0}{\lambda^2} \tag{9}$$

$$R = \lambda G A_0 \tag{10}$$

The expressions of $B$ and $R$ according to Muhr's theory can also be used within Equation (3) to evaluate the horizontal bearing stiffness, by using the deformed length $h$ instead of $h_0$.

Figure 4(A) shows and compares the relationship between applied vertical load and vertical displacement according to the Equations (2), (6) and (8). In the same figure, the curve obtained numerically by Orfeo et al.[22] is shown for comparison (the axial load was not monitored during the experiments). It can be observed that Muhr's theory better captures the nonlinear trend of increase of stiffness with the compressive displacement.

Figure 4(B) compares the estimates of the initial shear stiffness at zero shear displacement for increasing values of the applied vertical displacement according to Muhr's theory, Stanton's theory, Gent,[40] and the experimental results. Since the theories provide estimates of the tangent shear stiffness at zero horizontal displacement, the shear modulus of the rubber material at 0% shear strain is considered, corresponding to $G = 0.63$ MPa (Figure 2B). In general, the horizontal stiffness reduces for increasing vertical load, and the condition of instability is attained when it becomes zero. Muhr's model provide an overall good estimate of the shear stiffness for increasing compression levels. It is also interesting to observe that the ratio between the initial horizontal and vertical stiffness is about 43, which is significantly lower than the values typical of high shape factor bearings (several hundred times,[2] e.g., about 800 for $S = 12$ in ref. 60, which deals with isolation bearings for bridges).

While the maximum compressive load considered experimentally is 29 kN, analytical formulations are also used for higher compression levels to estimate the buckling load. Table 1 illustrates the estimates of the buckling load according to Muhr, Stanton and Gent models. It can be observed that all the theories underestimate the buckling load of the bearing which is likely to achieve the buckling condition for a compressive load equal to 34 kN (obtained by extrapolation of the experimental results). However, Muhr's model provides a better estimate of the buckling load with an error of only 12%. Table 1 also illustrates the buckling load according to the numerical results provided by Orfeo et al.,[22] which is equal to 39 kN. It is worth observing, from the same

table, that the critical load according to the theory of Gent[40] is only 40% of the value extrapolated from the experiment.

In general, the bearings are expected to experience some rotation at the top and therefore a formulation is needed to describe their behaviour under rotation, as well as the coupled rotational-translation behaviour. For this purpose, similarly to Crowder et al.,[61] it is possible to refer to the work of Chang.[62] Denoting with $v_{b,top}$ and $q_{b,top}$, respectively, the translation and rotation at the top of the bearing, the following relationship can be used to relate these quantities to the shear force and bending moment applied at the top of the bearing ($V_{top}$ and $M_{top}$):

$$\begin{bmatrix} V_{top} \\ M_{top} \end{bmatrix} = \begin{bmatrix} k_x & k_{x,\theta} \\ k_{\theta,x} & k_\theta \end{bmatrix} \begin{bmatrix} v_{b,top} \\ \theta_{b,top} \end{bmatrix} = \frac{N}{2\tan\left(\frac{\alpha h}{2}\right) - \alpha\beta h} \begin{bmatrix} \alpha\beta & -\tan\left(\frac{\alpha h}{2}\right) \\ -\tan\left(\frac{\alpha h}{2}\right) & \frac{1}{\alpha\beta} - \frac{h}{\sin(\alpha\beta)} \end{bmatrix} \begin{bmatrix} v_{b,top} \\ \theta_{b,top} \end{bmatrix} \tag{11}$$

where $k_x$ is the horizontal stiffness (coincident with $k_h$ of Equation (3) for zero horizontal deflections), $k_q$ is the rotational stiffness and $k_{x,q}$ a coupling term.

Under strong earthquake inputs, elastomeric bearings undergo large lateral displacements, and the rubber is subjected to high shear strains. In order to capture these effects, reference can be made to Nagarajaiah et al.'s[47] extension of Koh and Kelly's mechanical model, which considers large displacements, large rotations, and nonlinearity of rubber. The change of the horizontal stiffness $k_x$ with the horizontal displacement $v_{top}$ is evaluated solving numerically the following system of equations:

$$\begin{cases} \frac{R}{h}\left(1 - C_s\left(\frac{s}{t_r}\right)\right) s = F\cos\varphi + N\sin\varphi + \frac{\pi^2 B}{h}\frac{C_\theta \varphi^2}{2} \\ \frac{\pi^2 B}{h}\left(1 - C_\varphi\left(\frac{s}{t_r}\right)\right)\varphi = N(h\sin\varphi + s\cos\varphi) + F(h\cos\varphi - s\sin\varphi) \\ v_{top} = h\sin\varphi + s\cos\varphi \end{cases} \tag{12}$$

where $F$ and $N$ are the horizontal and vertical force, the expressions of $R,B$, and $h$ are evaluated according to the considered theory, $C_s$ and $C_j$ are material parameters that describe their evolution for increasing nominal shear strain levels, and $j$ and $s$ are the rotation and the shear displacement in the Koh and Kelly's mechanical model, respectively. The system of equations is solved by finding the values of $s$, $j$ and $F$ for increasing values of $v_{top}$, and the horizontal secant stiffness $k_x$, corresponds to the ratio between $F$ and $v_{top}$. For small value of $s$ and $j$, $C_s = 0$ and $C_j = 0$, the system of equations reduces to the expression derived by Koh and Kelly.[33]

For describing the reduction of the vertical stiffness with the increase of the horizontal displacement, Warn et al.'s model has been adopted.[63] This model accounts for the drop in height of the bearing due to the horizontal displacement, whereas the change of the stiffness with the increase of the axial load is assumed negligible. The following expression taken from Warn et al.[63] can be used:

$$k_z = k_{z0}\frac{1}{\left[1 + \frac{3A_0}{I}\frac{v_{top}^2}{\pi^2}\right]} \tag{13}$$

where $k_{z0} = \partial N/\partial v_v$ is the vertical stiffness evaluated in correspondence of the bearing's deformed configuration under the applied compressive force $N$, and $I$ is the second moment of area of the bearing cross section.

To summarise, the analytical model of the LSF bearings used in the next section for the simulation of the dynamic response of the prototype uses the expression of the horizontal secant stiffness $k_x$ resulting from the solution of Equation (12), the expressions of the rotational stiffness $k_f$ and of the coupling between horizontal displacements and rotations $k_{x,f}$ reported in Equation (11), the expression of the vertical stiffness $k_z$ from Equation (13), with $k_{z0}$ derived by differentiation of Equation (8).
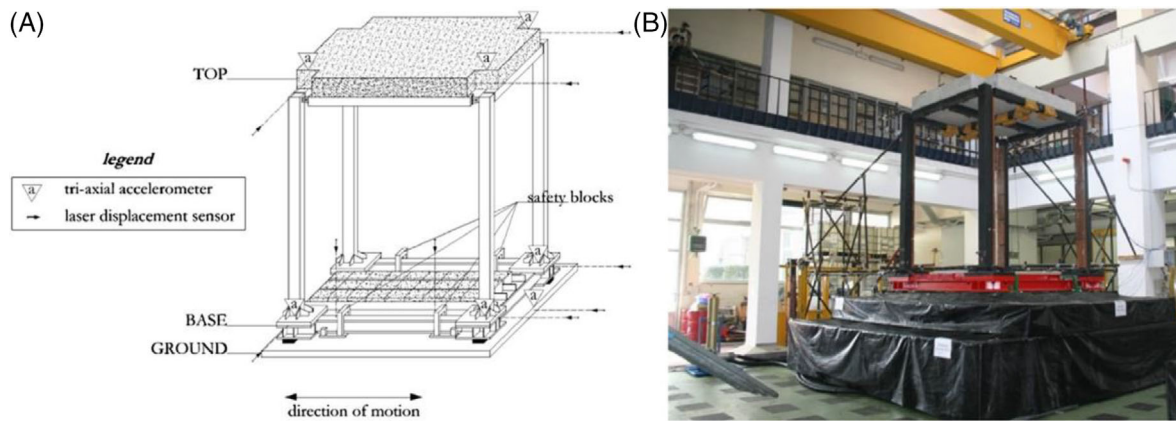
**FIGURE 5** (A) Cabinet projection of the prototype building and the instrumentation set-up; (B) view of the test frame of the shaking table at the DiST laboratory University of Naples Federico II.[66]

**TABLE 2** Identified dynamic properties of the isolated system.

| | Mode 1 | | Mode 2 | | Mode 3 | |
|---|---|---|---|---|---|---|
| | Test 1 | Test 2 | Test 1 | Test 2 | Test 1 | Test 2 |
| Vibration period [s] | 1.21 | 1.24 | 0.27 | 0.26 | 0.08 | 0.08 |
| Damping ratio [–] | 0.08 | 0.06 | 0.08 | 0.04 | 0.06 | 0.06 |

## 3 | SHAKING TABLE TESTS

### 3.1 | Prototype, tests description and dynamic identification

This subsection briefly describes the shaking table tests carried out in University of Naples Federico II on a building prototype mounted on the LSF bearings manufactured at TARRC.[41] Figure 5 illustrates the superstructure, which consists in a one storey steel frame, with plan dimensions of 2.65 × 2.15 m and total height 2.9 m. The columns have a box section 0.15 × 0.15 × 0.15 m, and they are connected to the base floor by means of a steel plate (0.61 × 0.45 m). The beams supporting the top slab are hot-formed square hollow sections 120 × 120 × 12.5 mm pinned to the columns. The four external beams at the base of the frame have HEM 160 profile. The mass of the base floor is equivalent to 3.6 tons, whereas the mass of the floor at the top is equal to 4.1 tons. The fixed-base structure has a fundamental period of vibration of $T_s = 0.24$ s. It is noteworthy that the same superstructure has been recently used to test alternative isolation systems such as recycled rubber and fibre-reinforced unbonded isolators.[64,65]

Table 2 summarizes the experimental frequencies, periods, and damping ratios of the system. These have been obtained by applying the Stochastic Subspace Identification (SSI) method,[67] using the recorded acceleration responses at the base and top level under two random input tests (i.e., Test 1, Test 2), with ground motions applied in the direction of the widest frame span. The tests induced a peak horizontal displacement of the bearings of 7.44 and 16.33 mm, respectively, corresponding to average shear strain of 13% and 29%.

The identified value of the fundamental vibration period is 1.21s, corresponding to an equivalent period of the full-scale structure of 2.1s (the prototype has a geometry scale factor of 1/3 and thus the period of the full scale structure is $\sqrt{3}$ times the period of the prototype). It is noteworthy that taking the superstructure as rigid and the bearings as infinitely stiff in the vertical direction, and using the initial bearing stiffness $k_{is} = 53$ kN/m evaluated in Subsection 2.3 under the axial load of 19 kN, an isolation period $2\pi\sqrt{M_{tot}/4k_{is}} = 1.21$s is obtained, which coincides with the experimental one.

After performing the random vibration tests, further tests were carried out under seven earthquake ground motions selected from the European strong-motion database, whose main characteristics are described in Table 3. The next

**TABLE 3** Ground motion characteristics.

| Waveform ID | Earthquake Name | Earthquake Country | Mw | PGA (m/s²) | PGV (cm/s) | PGD (cm) |
|---|---|---|---|---|---|---|
| 7142 | Bingol | Turkey | 6.3 | 2.55 | 18.29 | 3.25 |
| 55 | Friuli | Italy | 6.5 | 2.55 | 15.25 | 9.29 |
| 200 | Montenegro | Montenegro | 6.9 | 2.55 | 12.87 | 9.60 |
| 428 | Etolia | Greece | 5.3 | 2.55 | 12.46 | 6.06 |
| 372 | Lazio Abruzzo | Italy | 5.9 | 2.55 | 15.02 | 6.80 |
| 290 | Campano Lucano | Italy | 6.9 | 2.55 | 44.10 | 16.20 |
| 287 | Campano Lucano | Italy | 6.9 | 2.55 | 43.90 | 14.00 |

Abbreviations: Mw, magnitude; PGA, peak ground acceleration; PGD, peak ground displacement; PGV, peak ground velocity.
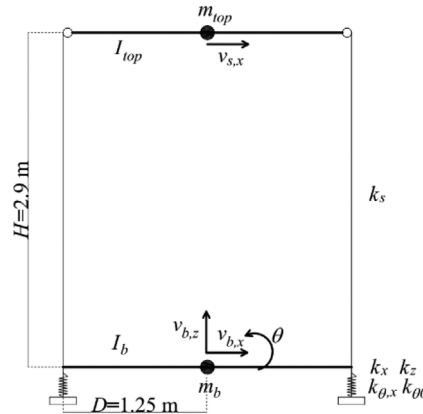


**FIGURE 6** Model of the base isolated structure.

subsection describes the development and validation of a numerical model for simulating the dynamic and seismic response of the isolated structure with LSF bearings.

## 3.2 | Simplified model

Since the shaking table test configuration has a plane of symmetry, only half of the building is modelled. Figure 6 illustrates the model representing the isolated frame building and the generalised coordinates that are considered for deriving the equations of motion of the system through the Lagrange's equations. The superstructure is simplified as a single degree of freedom system with mass $m_{\text{top}}$ and stiffness $k_s$, with the mass located at a distance $H$ from the supporting rigid base of mass $m_b$. The base, of width $2D$, is supported by two springs with horizontal, vertical and rotational stiffness denoted as $k_x$, $k_z$, $k_{x,\theta}$, respectively. These are assumed constant during the seismic motion. The generalised coordinates are: the rotation $\theta$ of the base (coincident with the rotation of the bearing top $\theta_{b,top}$), the vertical displacement of the base $v_{b,z}$ (coincident with the vertical displacement of the bearings), the horizontal displacement of the base $v_{b,x}$ (coincident with the bearings' top displacement $v_{b,top}$), and the horizontal displacement of the superstructure relative to isolation system $v_{s,x}$.

The kinetic energy and the potential energy of the system are defined as follows:

$$T = \frac{1}{2}m_b\left(\dot{v}_{b,x} + \dot{v}_{g,x}\right)^2 + \frac{1}{2}m_{top}\left(\dot{v}_{b,x} + \dot{v}_{g,x} + H\dot{\theta} + \dot{v}_{s,x}\right)^2 + \frac{1}{2}m_{tot}\left(\dot{v}_{b,z}\right)^2 + \frac{1}{2}I_b\dot{\theta}^2 + \frac{1}{2}I_{top}\dot{\theta}^2$$

$$V = 2\left(\frac{1}{2}k_x\left(v_{b,x}\right)^2 + \frac{1}{2}k_z\left(v_{b,z}\right)^2 + \frac{1}{2}k_z(\theta D)^2 + \frac{1}{2}k_{\theta 0}\theta^2 + \frac{1}{2}k_s v_{s,x}^2 + k_{\theta,x}v_{b,x}\theta + \frac{1}{2}k_{\theta,x}v_{b,x}^2\right) \tag{14}$$

where $v_{g,x}$ denotes the response induced by the earthquake ground motion $I_b$ and $I_{top}$ are the moment of inertia of mass $m_b$ and $m_{top}$, respectively.

The terms $k_{\theta,x}$, denotes the coupling between the horizontal displacement and the rotation.

The Lagrangian is therefore:

$$L = T - V = \frac{1}{2}m_b\left(\dot{v}_{b,x} + \dot{v}_{g,x}\right)^2 + \frac{1}{2}m_{top}\left(\dot{v}_{b,x} + \dot{v}_{g,x} + H\dot{\theta} + \dot{v}_{s,x}\right)^2 + \frac{1}{2}m_{tot}\left(\dot{v}_{b,z}\right)^2 +$$

$$+\frac{1}{2}I_b\dot{\theta}^2 + \frac{1}{2}I_{top}\dot{\theta}^2 - k_x v_{b,x}{}^2 - k_z v_{b,z}{}^2 - k_z(\theta D)^2 - k_{\theta 0}\theta^2 - k_s v_{s,x}^2 - 2k_{\theta,x}v_{b,x}\theta - k_{\theta,x}v_{b,x}{}^2 \quad (15)$$

The corresponding Euler-Lagrange equations of motion are obtained by the following derivatives of the Lagrangian:

$$\begin{aligned}
\frac{\partial}{\partial t}\left(\frac{\partial L}{\partial \dot{v}_{b,x}}\right) - \frac{\partial L}{\partial v_{b,x}} &= 0 \\
\frac{\partial}{\partial t}\left(\frac{\partial L}{\partial \dot{\theta}}\right) - \frac{\partial L}{\partial \theta} &= 0 \\
\frac{\partial}{\partial t}\left(\frac{\partial L}{\partial \dot{v}_{s,x}}\right) - \frac{\partial L}{\partial v_{s,x}} &= 0 \\
\frac{\partial}{\partial t}\left(\frac{\partial L}{\partial \dot{v}_{b,z}}\right) - \frac{\partial L}{\partial v_{b,z}} &= 0
\end{aligned} \quad (16)$$

which gives:

$$\begin{cases}
m_b\left(\ddot{v}_{b,x} + \ddot{v}_{g,x}\right) + m_{top}\left(\ddot{v}_{b,x} + \ddot{v}_{g,x} + H\ddot{\theta} + \ddot{v}_{s,x}\right) + 2k_x v_{b,x} + 2k_{\theta,x}v_{b,x} + 2k_{\theta,x}\theta = 0 \\
m_{top}H\left(\ddot{v}_{b,x} + \ddot{v}_{g,x} + H\ddot{\theta} + \ddot{v}_{s,x}\right) + I_b\ddot{\theta} + I_{top}\ddot{\theta} + 2k_z D^2\theta + 2k_{\theta 0}\theta + 2k_{\theta,x}v_{b,x} = 0 \\
m_{top}\left(\ddot{v}_{b,x} + \ddot{v}_{g,x} + H\ddot{\theta} + \ddot{v}_{s,x}\right) + 2k_s\left(v_{s,x}\right) = 0 \\
m_{tot}\ddot{v}_{b,z} + 2k_z\left(v_{b,z}\right) = 0
\end{cases} \quad (17)$$

The response of the structure to earthquake-induced ground motion $\ddot{v}_g(t)$, when also damping is included, can be described by the differential equation in matrix form:

$$\mathbf{M}\ddot{\mathbf{v}} + \mathbf{C}\dot{\mathbf{v}} + \mathbf{K}\mathbf{v} = -\mathbf{M}\mathbf{I}\ddot{v}_g \quad (18)$$

where $\mathbf{I}$ is the influence vector and the matrices are defined as follows:

$$\mathbf{I} = \begin{bmatrix} 1 \\ 0 \\ 0 \\ 0 \end{bmatrix} \quad (19)$$

$$\mathbf{v} = \begin{bmatrix} v_{b,x} \\ \theta \\ v_{s,x} \\ v_{b,z} \end{bmatrix} \quad (20)$$

$$\mathbf{M} = \begin{bmatrix} m_b + m_{top} & m_{top}H & m_{top} & 0 \\ m_{top}H & m_{top}H^2 + I_b + I_{top} & m_{top}H & 0 \\ m_{top} & m_{top}H & m_{top} & 0 \\ 0 & 0 & 0 & m_b + m_{top} \end{bmatrix} \quad (21)$$

$$\mathbf{K} = \begin{bmatrix} 2k_x & 2k_{\theta,x} & 0 & 0 \\ 2k_{\theta,x} & 2k_z D^2 + 2k_{\theta 0} & 0 & 0 \\ 0 & 0 & 2k_s & 0 \\ 0 & 0 & 0 & 2k_z \end{bmatrix} \quad (22)$$

**TABLE 4** Base isolated system parameters.

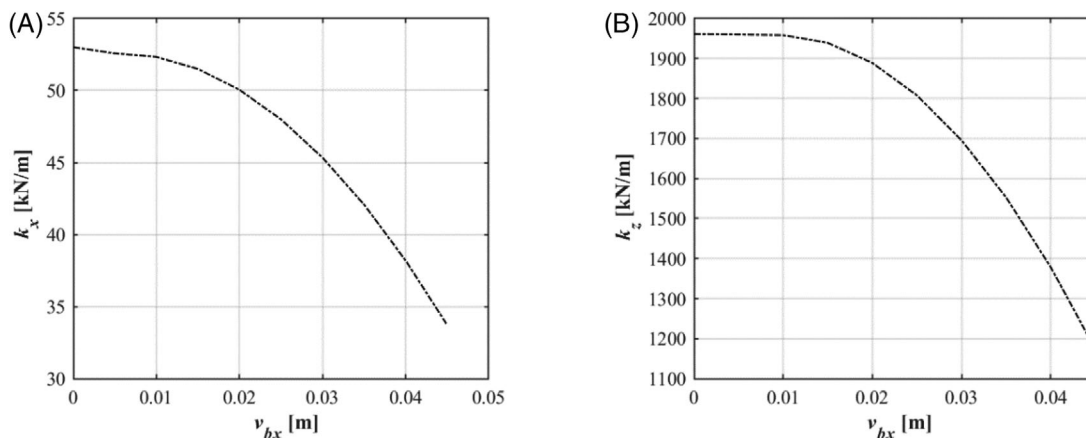| $I_b$ [m⁴] | $I_{top}$ [m⁴] | $m_b$ [ton] | $m_{top}$ [ton] | $k_{x0}$ [kN/m] | $k_{z0}$ [kN/m] | $k_{\theta 0}$ [kNm] | $k_{x\theta}$ [kNm] | $c_b$ [Ns/m] |
|---|---|---|---|---|---|---|---|---|
| 1.22 | 1.98 | 1.26 | 2.05 | 1939 | 53 | 0.0032 | 0.5 | 2.88 |



**FIGURE 7** Variation with the horizontal displacement of the secant horizontal stiffness (A) and of the vertical stiffness (B).

The damping matrix **C** can be constructed in a simplified way by assuming a value for the damping ratio of the base isolation system and of superstructure $\xi_b$ and $\xi_s$ as follows:

$$\mathbf{C}(1,1) = c_b = 2\xi_b \frac{\mathbf{K}(1,1)}{\omega_{is}} \tag{23}$$

$$\mathbf{C}(3,3) = c_s = 2\xi_s \frac{\mathbf{K}(3,3)}{\omega_{is}} \tag{23}$$

The adopted value of $\xi_b$ refers to the equivalent damping ratio of the bearing corresponding to a nominal shear strain of 80% (Figure 2C). This is the ratio between the maximum horizontal displacement experienced by the bearing due to the Bingol earthquake and the total rubber layers' height. The damping ratio of the superstructure $\xi_s$ is assumed equal to 0.65%.[68] The natural frequency $\omega_{is}$ is known from the eigenvalue analysis. Table 4 shows the values of the masses and moments of inertia considered in this study along with the values of the initial stiffness and damping of the bearing. The vertical and horizontal stiffness are determined by considering Muhr's theory[39] for the bearing compressed by a vertical load of 19 kN. In particular, $k_{x0}$ is obtained from Equation (3), and $k_{z0}$ by differentiation of the expression of $N$ in Equation (8). The expression of the rotational stiffness $k_{\theta 0}$ and of the coupling term $k_{x\theta}$ can be found in Equation (11) and are assumed constant.

The horizontal stiffness variation with horizontal displacement is defined by solving Equation (12) as discussed in the previous section, with $B$ and $R$ from the theory of Muhr[39] and $C_s$ and $C_j$ calibrated against the experimental double-shear test results and assumed equal to 0.14. The vertical stiffness reduction is evaluated using Equation (13). The coupling term is assumed not to change with the horizontal displacement.

Figure 7 shows the variation of the horizontal and vertical stiffnesses with the horizontal displacement up to 45 mm (i.e., the maximum deflection experienced by the bearing during Bingol earthquake) according to Equations (12) and (13) for an axial load of 19 kN.

The undamped modal properties of the system can be found by solving the eigenvalue problem

$$\det[\mathbf{K} - \omega_n{}^2\mathbf{M}] = 0 \tag{24}$$

Figure 8 illustrates the modal shapes of the horizontal vibration modes of the model, by showing the values of the displacements $v_{b,x}$, $v_{s,x}$ and $\theta H$, normalised by the maximum horizontal displacement for each mode. It can be observed
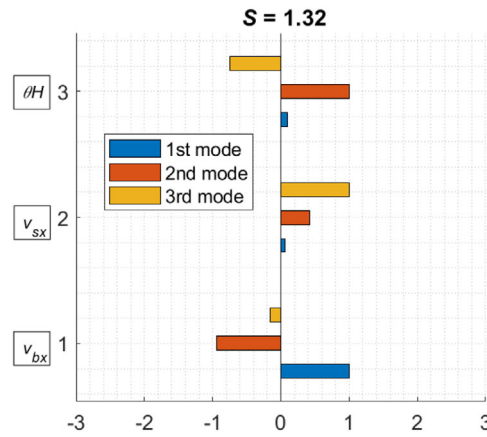
**FIGURE 8** Modal shapes of the first three modes of vibration.

**TABLE 5** Periods of vibration, mode shapes and MAC values.

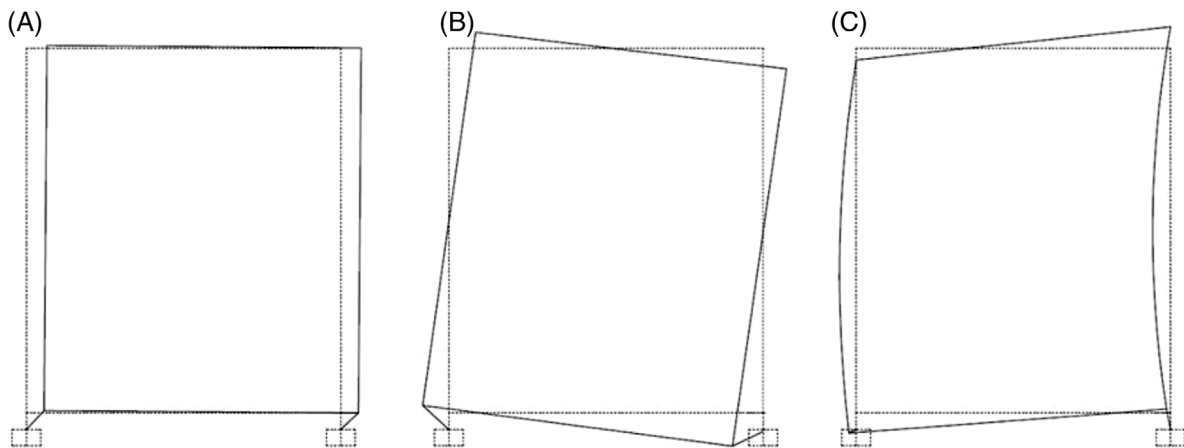| Mode | First | Second | Third |
|---|---|---|---|
| Natural periods [s] | 1.25 | 0.28 | 0.08 |
| MAC | 0.99 | 0.96 | 0.86 |



**FIGURE 9** Mode shapes of the base isolated structure. (A) First mode, (B) Second mode, (C) Third mode.

that there is a small amount of rocking in the first mode, whereas there is a higher contribution in the second and third mode. Table 5 shows the natural periods evaluated at each mode showing a good agreement with those estimated via the dynamic identification (Table 2). Furthermore, the Modal Assurance Criterion (MAC)[68] has been used to compare the mode shapes derived from the analytical model with those obtained experimentally. The obtained MAC values, shown in Table 5, indicate that mode shapes 1 and 2 are almost identical with the experiment ones (MAC higher than 0.9) whereas a slight difference (MAC between 0.8 and 0.9) can be found for mode 3. Figure 9 presents the deflection shapes corresponding to the first three horizontal modes. The first mode is primarily dominated by the horizontal deflections of the bearing, with the superstructure moving almost rigidly. The second mode involves significant deflections of the bearings, as well as base rotation and superstructure deflections. The third modal shape is controlled mainly by the rotation of the base and by the deflection of the columns.

In order to analyse the response of the isolated system to the seismic inputs, a numerical method based on a fourth-order Runge-Kutta algorithm was employed. In particular, the second-order differential equation of motion corresponding to
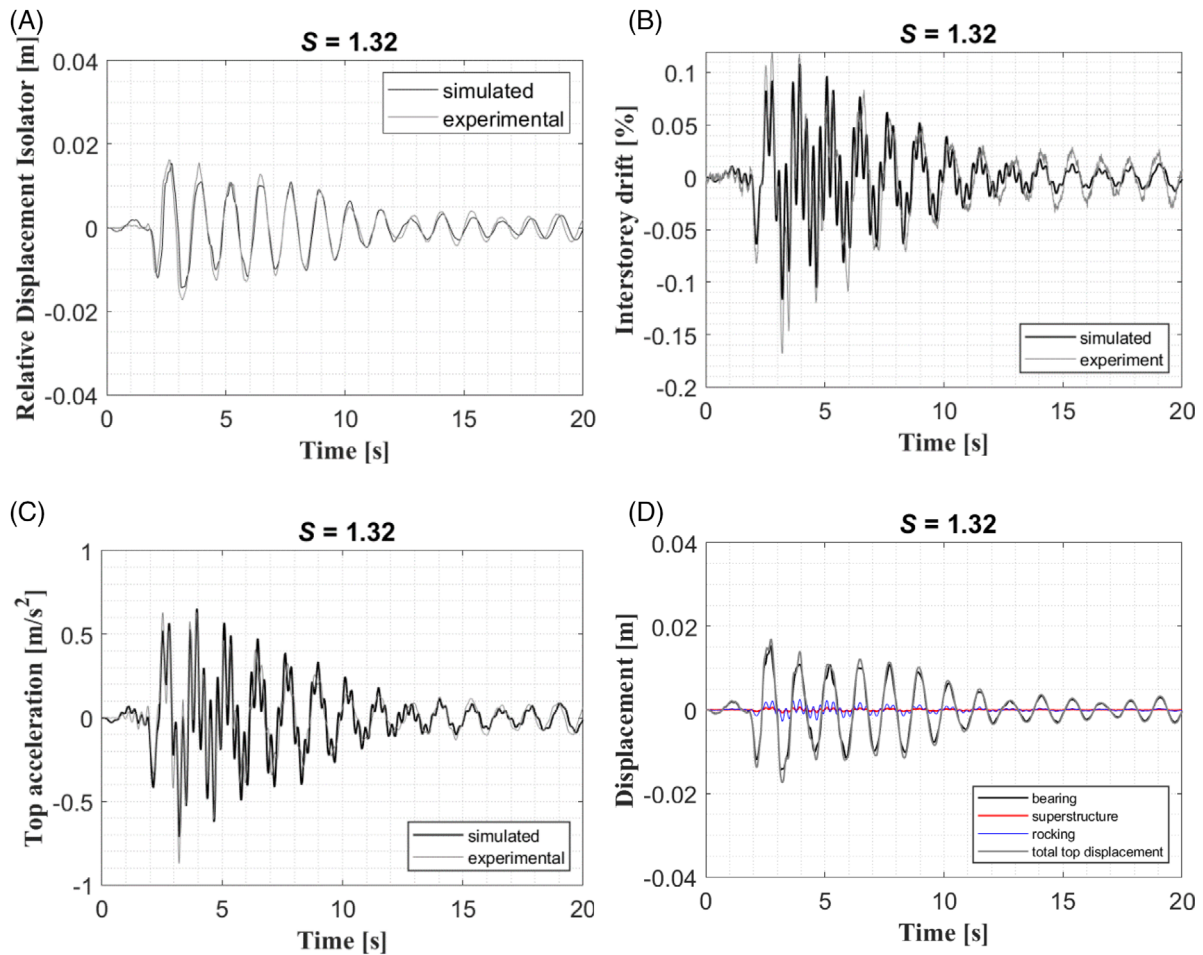
**FIGURE 10** Response to Friuli earthquake. (A) Relative displacement isolator time history, (B) Interstorey drift, (C) Acceleration at the top node, (D) Time history of the bearing, superstructure and rocking contributions to the top node displacement.

Equation (18) was rewritten as a first-order one, and solved using the "ode45" function in Matlab.[70] To simplify the model and avoid the simultaneous solution of algebraic and differential equations, the value of the secant stiffness in the vertical and transverse direction corresponding to the maximum displacement and the value of the axial force due to permanent load was used. The secant stiffness was determined by solving externally the algebraic equations iteratively (11) to (13). Once the secant stiffness values (i.e., both horizontal and vertical) were determined, the ODEs were iteratively solved with constant stiffness values throughout the seismic analysis, starting from the initial ones. The stiffness values were updated based on the bearing displacements until convergence was achieved on the bearing maximum displacement. Although the concept of secant stiffness is widely employed for seismic analyses, it should be noted that it may have some impact on the accuracy of the results. However, considering at each time step the actual bearing resisting forces in the horizontal and vertical direction, that are a function of the current bearing displacement, does not yield improved results. This may be due to other simplifying assumptions inherent to the model, for example, that the vertical bearing stiffness is independent of the variation of axial loading. Further refinements are required to improve the accuracy of the bearing model, which are, however, out of the scope of this study. Figure 10(A)–(C) compare the experimental and numerical response under Friuli record, in terms of horizontal bearing displacement (Figure 10A), superstructure interstorey drift (Figure 10B) and acceleration at the top of the superstructure (Figure 10). In general, a good agreement is observed between the experimental and the numerical response. Figure 10(C) illustrates the contribution to the displacement response of the top node by the horizontal deflections of the bearings, the superstructure deflection, and the rocking contribution. The rocking contribution is the rotation experienced by the base isolation system under seismic load multiplied by the height of the superstructure $H$. It can be observed that the displacements are all in phase, suggesting mode 1 predominates the response, and the superstructure response is dominated by the bearing deflection. The rocking of the bearings contributes to less than 16% of the peak top displacement of the structure, despite the relatively high vertical flexibility of the LSF
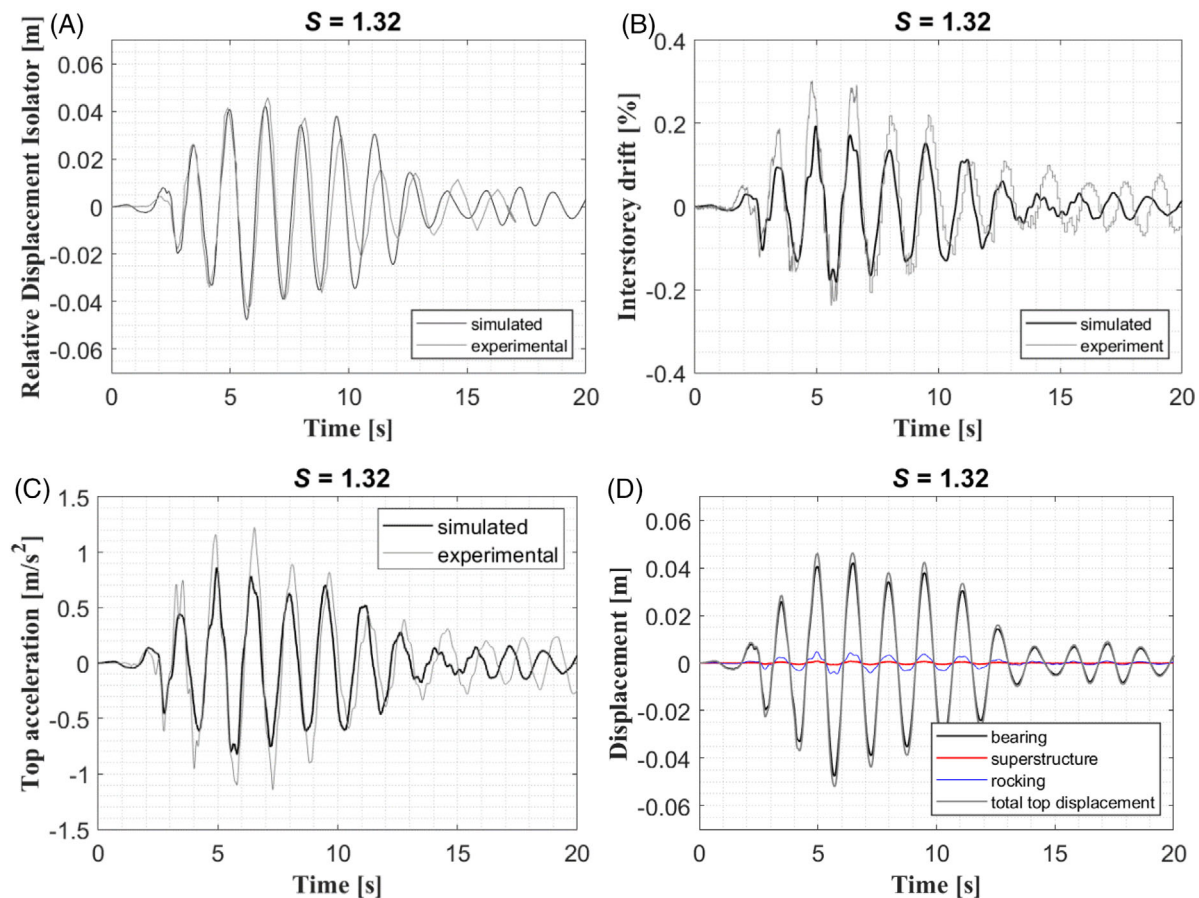
**FIGURE 11**  Response to Bingol earthquake. (A) Relative displacement isolator time history, (B) Interstorey drift, (C) Acceleration at top node and (D) Time history of the bearing, superstructure and rocking contributions to the top node displacement.

bearings, compared to bearings with high shape factors. This outcome is in line with previous findings demonstrating that a vertical frequency higher than 1–3 Hz provides negligible rocking motion and results into a fundamental horizontal deflection mode of the structure.[20,71] Recently Losanno et al. found that even in the case of fibre-reinforced elastomeric isolators a limited axial-to-horizontal stiffness ratio would not affect the effectiveness of base isolation under seismic motion.[72]

Figure 11(A–C) shows the results obtained for the Bingol earthquake, which induces higher deflections of the bearings compared to the other records. The agreement between the experimental and analytical results for both the relative displacement of the isolator and the interstorey drift satisfactory up to approximately 8 s, at which point the amplitude of the input ground motion decreases and the differences between the test and model become more significant. This may be due to a limitation in the modelling approach, specifically the assumption of using a single secant value for the reduced horizontal and vertical stiffnesses. In reality, the horizontal and vertical stiffness of the bearings exhibit a more complex, nonlinear variation during the loading history, especially when instability is approached. Developing an analytical model for simulating this is out of the scope of the present study. It is noteworthy that to properly simulate the response to Bingol earthquake input and the period elongation that characterises the response under the large amplitudes of vibrations, it is necessary to consider the horizontal and vertical stiffness reduction for increasing horizontal displacements, as shown in Figure 7(A, B).

It is worth mentioning that significant differences can be observed in the drift responses. Orfeo et al.[22] discussed this discrepancy, attributing it to the flexibility in the connection between the superstructure and the base, which was assumed to be rigid in the numerical model. Notably, the results obtained from the simplified model are more consistent with those presented in Orfeo et al.[22] The numerical model exhibits a maximum drift that is only 6% greater than that of the simplified model. The acceleration at the top of the superstructure is another parameter that is affected by the superstructure modelling assumptions (including the damping). Nevertheless, the simplified numerical model provides results quite close to
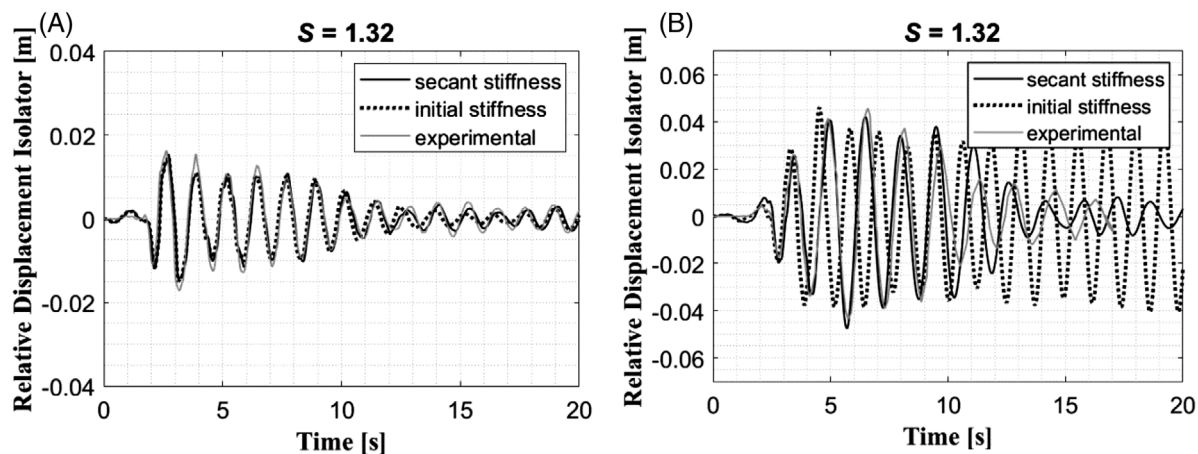
**FIGURE 12** Relative displacement isolator time history: comparison between experiment, simplified model using the initial horizontal and vertical stiffness and the simplified model using secant horizontal and vertical stiffness under (A) Friuli earthquake input and (B) Bingol earthquake input.

**TABLE 6** Maximum absolute values of various response parameters according to experimental test and numerical model.

| | Max displacement isolator [m] | | | Max drift structure [%] | | | Max top acceleration [m/s$^2$] | | |
| --- | --- | --- | --- | --- | --- | --- | --- | --- | --- |
| Earthquake name | Exp | Numerical model | Relative error % | Exp | Numerical model | Relative error % | Exp | Numerical model | Relative error % |
| Bingol | 0.0459 | 0.0466 | 1.6 | 0.3 | 0.23 | −24.5 | 1.2 | 0.86 | −28 |
| Friuli | 0.0172 | 0.0158 | −9.4 | 0.17 | 0.13 | −24.1 | 0.9 | 0.71 | −20 |
| Montenegro | 0.0173 | 0.0188 | 8.8 | 0.17 | 0.14 | −19.7 | 0.9 | 0.77 | −11.4 |
| Etolia | 0.0174 | 0.019 | 9.0 | 0.17 | 0.14 | −17.4 | 0.9 | 0.77 | −11.0 |
| Lazio/Abruzzo | 0.0176 | 0.019 | 8.3 | 0.16 | 0.14 | −13.2 | 0.9 | 0.78 | −10.3 |
| ID 290 | 0.0176 | 0.019 | 8.1 | 0.16 | 0.14 | −15.8 | 0.9 | 0.78 | −9.9 |
| ID 287 | 0.0173 | 0.0189 | 9.2 | 0.17 | 0.14 | −19.2 | 0.9 | 0.78 | −10.0 |

those obtained with the advanced numerical model. The acceleration obtained from the numerical model is 16% greater than that of the simplified model.

Figure 11(D) illustrates the three contributions to the top displacement response, showing again that these contributions are all in phase and that the rocking of base has a negligible effect on the response.

It is worth noting that incorporating the variation of vertical and horizontal stiffness with horizontal displacement according to Equations (12) and (13), leads to significantly improved results compared to those obtained by neglecting the stiffness variation. Figure 12(A, B) shows the time history response of the bearings in terms of relative horizontal displacement under Friuli and Bingol earthquakes, according to the numerical models with initial and secant stiffness values, and the experimental results. The model with reduced secant bearing stiffness is significantly more accurate, particularly under conditions of large displacement demand as in the case of Bingol earthquake.

Table 6 compares the experimental and numerical maximum absolute values of the isolator deflection, interstorey drift and acceleration at top for all the records. It is noteworthy that these results have been obtained considering the initial values of the horizontal and vertical bearing stiffness (Table 4) for all the analyses with the exception of the one considering Bingol record. For this record, the secant values of the horizontal and vertical stiffness have been considered. These are equal to 33 and 1180 kN/m, corresponding to a reduction of, respectively, 38% and 39% with respect to the initial values.

It can be observed that the numerical model describes accurately the response of the isolator with only 10% of relative error with respect to the experimental results (minimum error of 1.6% under Bingol record corresponding to largest isolator displacement), whereas a higher relative error (24%) can be observed for the prediction of maximum interstorey drift of the superstructure. In terms of top acceleration, the numerical model describes the Bingol response with 28% of relative error, which is due to the assumption of a secant horizontal stiffness (i.e., equivalent linear model) of the superstructure, whereas lower relative errors can be observed under the other records.

**TABLE 7** Horizontal and vertical stiffness of the bearings.

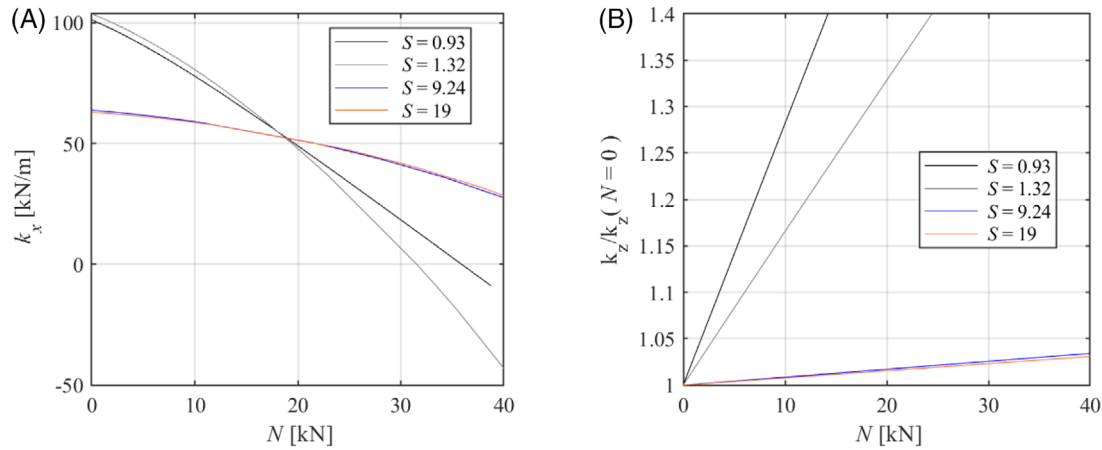| Shape factor $S$ | Initial horizontal Stiffness $k_{x0}$ [kN/m] | Initial vertical Stiffness $k_{z0}$ [kN/m] | $k_{z0}/k_{x0}$ | Horizontal Period [s] | Vertical Period [s] |
|---|---|---|---|---|---|
| 0.90 | 53 | 1310 | 25 | 1.25 | 0.24 |
| 1.32 | 53 | 1913 | 37 | 1.25 | 0.20 |
| 9.24 | 53 | 31745 | 608 | 1.24 | 0.05 |
| 19 | 53 | 127120 | 2434 | 1.24 | 0.02 |



**FIGURE 13** Effect of the vertical load on (A) horizontal stiffness and (B) vertical stiffness, for different shape factors.
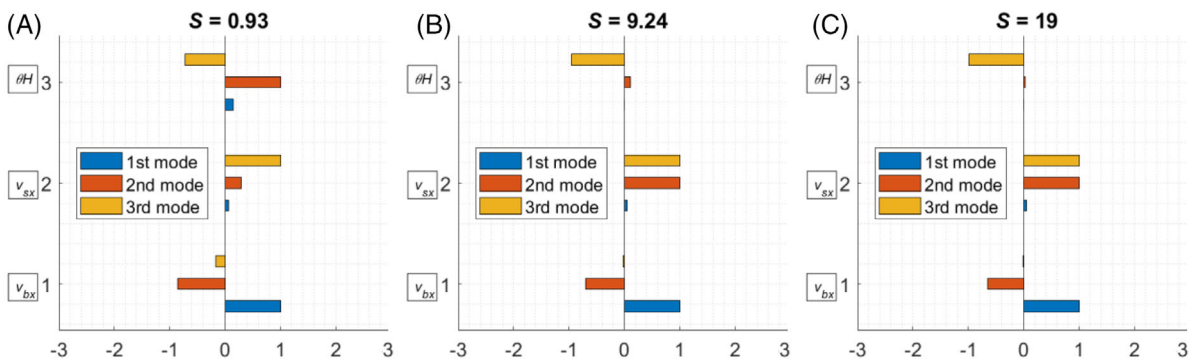


**FIGURE 14** Mode shapes of the first three modes of vibration for the three designed bearing: (A) $S = 0.93$, (B) $S = 9.56$ and (C) $S = 10$.

# 4 | PARAMETRIC STUDY

This section investigates the seismic response of a set of models that are obtained from the model investigated in the previous section by varying the shape factor of the bearings. Table 7 describes the geometric and mechanical properties of the bearings, which have been designed in order to obtain the same horizontal stiffness exhibited under the permanent load of 19 kN. The initial horizontal and vertical stiffness have been estimated using Muhr's theory.

It can be noted that the vertical period reduces significantly with the increase of the shape factor, whereas the first isolation period is not affected, since it is mainly controlled by the horizontal stiffness of the bearings. Figure 13 illustrates the variation of the initial horizontal and vertical stiffness of the different bearings for increasing values of the vertical load.

Figure 14 describes the contributions of the various Lagrangian parameters to the shapes of the first three modes, for the various values of $S$ considered. The system with $S = 0.9$ exhibits modal shapes very similar to those of the system with $S = 1.32$. With the increase of $S$, the contribution of the rotational component in mode 1 and 2 reduces and disappears for
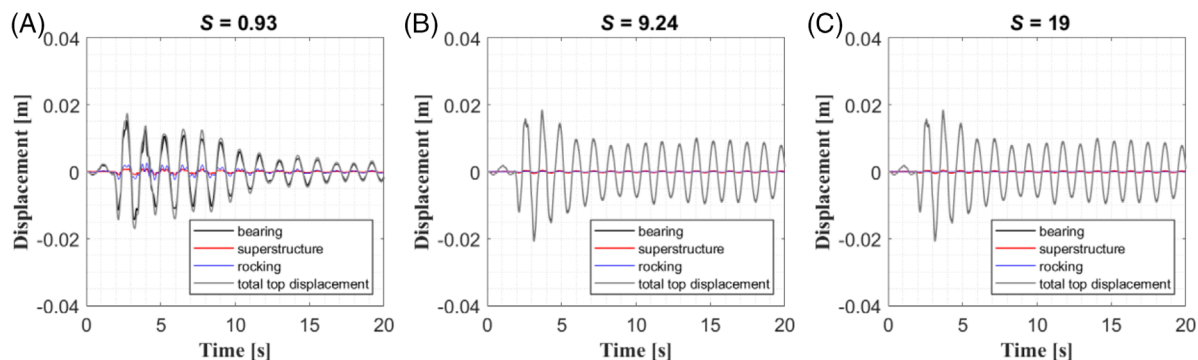
**FIGURE 15**  Response of Friuli earthquake: Time history of the bearing, superstructure and rocking contributions to the top node displacement: (A) $S = 0.93$, (B) $S = 9.56$, (C) $S = 19$.
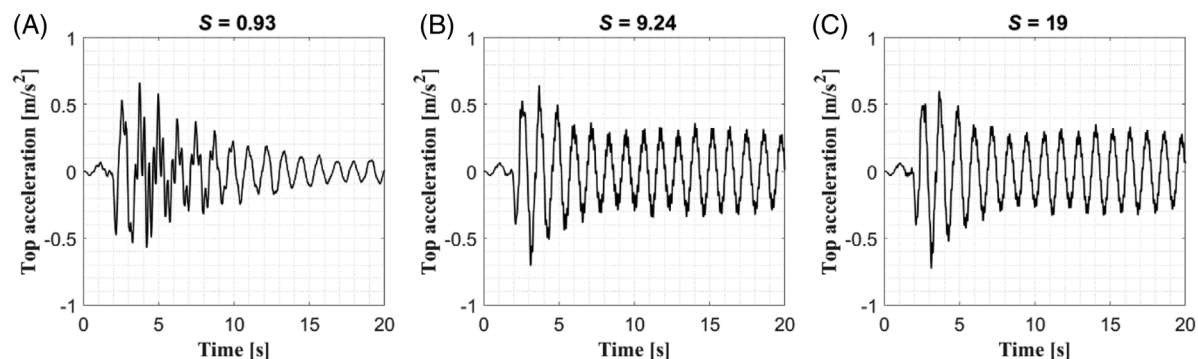


**FIGURE 16**  Response of Friuli earthquake in terms of top acceleration: (A) $S = 0.93$, (B) $S = 9.56$, (C) $S = 19$.

**TABLE 8**  Response of Friuli earthquake: Maximum isolator displacement, maximum total displacement at the top and rocking contribution.

| Shape factor $S$ [–] | Max Isolator displacement [m] | Max total top displacement [m] | Rocking contribution [m] | Rocking / Max Total Top displ [%] | Max Top Acceleration [m/s²] |
|---|---|---|---|---|---|
| 0.93 | 0.0155 | 0.0179 | 0.029 | 16.0 | 0.66 |
| 1.32 | 0.0158 | 0.018 | 0.028 | 15.7 | 0.71 |
| 9.56 | 0.019 | 0.0202 | 0.001 | 0.5 | 0.72 |
| 19 | 0.019 | 0.0203 | 0.0003 | 0.15 | 0.73 |

$S = 9.24$. This is due to the fact that with the increase of shape factor, the ratio $k_z/k_x$ increases as shown in Table 7 and this limits the rotation of the base slab.

The second part of the parametric study investigates the seismic response of the isolated systems models corresponding to bearings with different $S$ values. In the analyses, all the earthquake inputs of Table 3 were considered, with the exception of Bingol. Under these records, the response can be estimated assuming no variation in horizontal and vertical stiffness with the horizontal displacement. This removes the uncertainties related to the evaluation of the coupled horizontal-vertical behaviour of the bearings under larger displacements as those induced by Bingol. Figure 15(A–C) shows the time history of the top displacement responses for the case of Friuli earthquake input. Plotted in the same figures are the contributions to the displacement response of the top node by the bearings, the superstructure, and the rocking base. Figure 16(A–C) shows the response in terms of top acceleration under Friuli earthquake. Table 8 shows the maximum isolator displacement, the maximum displacement at the top of the superstructure, the rocking contribution due to the Friuli earthquake input and the maximum top acceleration. The total displacement demand and the maximum top acceleration increase slightly for increasing values of $S$, whereas the rocking contribution follows an opposite trend. In any case, the contribution of rocking to the top displacement response is about 16% for LSFs and reduces to 0.15% for the highest shape factor considered in this study.

**TABLE 9** Response of all earthquake inputs: Maximum total displacement at the top and rocking contribution.

| Shape factor S | 0.93 | | 1.32 | | 9.56 | | 19 | |
|---|---|---|---|---|---|---|---|---|
| Earthquake name | Max total top displ. [m] | Rocking / max top displ [%] | Max total top displ. [m] | Rocking / max top displ [%] | Max total top displ. [m] | Rocking / max top displ [%] | Max total top displ. [m] | Rocking / max top displ [%] |
| Friuli | 0.0179 | 16.0 | 0.018 | 15.7 | 0.0203 | 0.5 | 0.0203 | 0.15 |
| Montenegro | 0.0207 | 15.0 | 0.0216 | 14.7 | 0.0235 | 0.6 | 0.0235 | 0.15 |
| Etolia | 0.0208 | 14.9 | 0.0217 | 14.7 | 0.0236 | 0.6 | 0.0237 | 0.14 |
| Lazio/Abruzzo | 0.0207 | 15.0 | 0.0217 | 14.6 | 0.0237 | 0.6 | 0.0237 | 0.14 |
| ID 290 | 0.0208 | 15.0 | 0.0216 | 14.8 | 0.0236 | 0.6 | 0.0237 | 0.14 |
| ID 287 | 0.0207 | 15.0 | 0.0217 | 14.7 | 0.0235 | 0.6 | 0.0236 | 0.14 |

**TABLE 10** Response of all earthquake inputs: Maximum top acceleration [m/s$^2$].

| Shape factor S | 0.9 | 1.32 | 9.56 | 19 |
|---|---|---|---|---|
| Earthquake Name | | | | |
| Friuli | 0.664 | 0.714 | 0.719 | 0.733 |
| Montenegro | 0.756 | 0.765 | 0.814 | 0.791 |
| Etolia | 0.749 | 0.772 | 0.819 | 0.786 |
| Lazio/Abruzzo | 0.747 | 0.775 | 0.817 | 0.789 |
| ID 290 | 0.747 | 0.779 | 0.816 | 0.794 |
| ID 287 | 0.746 | 0.778 | 0.824 | 0.787 |

Table 9 reports the total displacement of the top of the superstructure and the rocking contribution resulting from the analyses carried out considering the various earthquake inputs. The rocking contribution exhibits the same decreasing trend for increasing values of the shape factor for the various earthquake inputs. A maximum ratio of the rocking to the maximum total displacement of 16% is obtained for the lowest shape factor, whereas a minimum ratio of 0.13% is observed for $S = 19$. The order of magnitude of the rocking contribution observed in the worst-case scenario is overall quite low. The maximum displacement at the top increases by 11% for Friuli earthquake and by 8% for the remaining earthquakes for values of $S$ increasing from 0.9 to 19. Finally, Table 10 reports the response of all earthquake input in terms of maximum top acceleration. In terms of effectiveness of base isolation, it can be observed that top acceleration increases with the increase of the shape factor. By including rocking component under horizontal excitation demonstrated in fact that LSF bearings enhance seismic performance of the isolation systems in comparison with higher shape factor bearings. This outcome is confirmed by displacement (Figure 15) and acceleration trend (Figure 16) demonstrating a lower number of peaks with lower magnitude in case of LSF bearings. Even if rocking contribution to top displacement is higher in case of LSF compared to higher shape factors, total top displacement and acceleration tend to reduce achieving a main advantage of base isolation in the former case.

## 5 | CONCLUSIONS

This study investigates experimentally and numerically the mechanical behaviour of laminated elastomeric bearings with a LSF and the dynamic response of structures mounted on them.

A simplified theory for describing the mechanical behaviour of LSF bearings under compressive and shear loadings is illustrated. The proposed theory is an extension of the theory of Muhr for slender blocks and, similar to the theory of Stanton, accounts for the important effects of axial shortening and rubber layer bulging on the bearing behaviour. The experimental tests conducted at TARRC rubber research centre on LSF rubber bearings with low damping and double shear testpieces are considered for validating the proposed theory and comparisons are also made also with the theories of Koh and Kelly and Stanton. Moreover, the shaking table tests carried out at University of Naples Federico II on the bearings manufactured at TARRC are also considered to show the application of the bearing model for the purpose of evaluating the dynamic behaviour and seismic response of structures mounted on LSF bearings.

With regards to the theories for describing the mechanical behaviour of LSF bearings, the following conclusions can be drawn:

- Linear theories as the one developed by Gent and Koh and Kelly for simulating the behaviour of isolation bearings with high shape factors cannot be used for the LSF considered in this study.
- Stanton's model, which accounts for the increase of plane area of the bearing due to compression, provides more accurate results estimates of the compressive and horizontal behaviour than the theories of Gent and Koh and Kelly.
- The formulation recently developed by Muhr, accounting for the change of height and area of the rubber layers under compression and also based on a finite strain formulation, provides the best fit to the experimental responses to compressive and horizontal loading.

The second part of the paper illustrates the results of the shaking table tests performed at University of Naples Federico II on a structural prototype isolated on the LSF bearings developed at TARRC. These results are complemented by the outcomes of the simulations carried out with a simplified model derived considering few generalized coordinates and based on the bearing model illustrated in the first part of the study.

The following conclusions are drawn:

- The simplified model based on very few generalized coordinates yields very good estimates of the system modal properties.
- The eigenvalues analysis shows that rocking of the base affects significantly only the second and third mode of vibration of the system.
- The proposed model provides accurate estimates of the seismic response of the isolated structure. The error in the estimation of the maximum bearing deflections is less than 10%, whereas higher errors are associated with the estimates of the superstructure drifts.
- The reduction of horizontal and vertical stiffness of the bearings for increasing horizontal displacements has to be considered to accurately capture the period elongation and the changes in dynamic behaviour of the system under the Bingol record, which induces larger deflections in the bearings compared to the other records.

In the final part of the paper, a parametric study is carried out to identify the effect of the bearing the shape factor on the dynamic behaviour of the isolated system. Based on the results of the analyses, the following conclusion can be drawn:

- To completely suppress the rocking motion, higher shape factor bearings are needed. However, the bearings with LSF perform better in terms of deflection of the base isolation system and of the superstructure in conjunction with lower acceleration.
- The contribution of the base rotation to the top displacement of the prototype is low even for the case of the lowest shape factor (16% for the Friuli earthquake).

Based on these results, it can be concluded that the proposed LSF bearing model can be used for preliminary assessment and design purposes and that rocking may not be significant even for low values of the shape factor of the isolation bearings. It is worth noting, however, that the proposed model has some limitations, particularly in cases where the bearing experiences large displacements such that the response cannot be described by considering the initial stiffness in the horizontal and transverse direction. For such instances, further experimental tests would be required to calibrate more accurate models for describing the non-linearities arising from material or geometric factors and the coupling between the horizontal and vertical responses. These experiments will have to be conducted under both quasi-static and dynamic loading, in order to shed light on the different behaviour expected under these conditions. In order to gather experimental data for validation of analytical and numerical models, in a future study load cells should be used to measure the horizontal and vertical loads acting on each single bearing. Future studies need to be carried out to extend the model developed by Muhr for describing the mechanical behaviour of LSF bearings with high damping rubber compounds and to evaluate its suitability under even larger bearing deflections.

University of Naples Federico II. The authors are also grateful to Giovanni Cuomo and Robert Picken who assisted with the bearing manufacturing and shaking table tests.

## DATA AVAILABILITY STATEMENT

The data that support the findings of this study are available from the corresponding author upon reasonable request.

## ORCID

*Alessandra Orfeo* 🄳 https://orcid.org/0000-0001-6072-7015

## REFERENCES

1. Kelly JM. *Earthquake-Resistant Design with Rubber*. Springer; 1993.
2. Konstantinidis D, Kelly J. *Mechanics of Rubber Bearings for Seismic And Vibration Isolation*. Wiley; 2013.
3. Constantinou M, Kartoum A, Kelly J. Analysis of compression of hollow circular elastomeric bearings. *Eng Struct*. 1992;14(2):103-111. doi:10.1016/0141-0296(92)90036-p
4. Montuori G, Mele E, Marrazzo G, Brandonisio G, De Luca A. Stability issues and pressure–shear interaction in elastomeric bearings: the primary role of the secondary shape factor. *Bull Earthquake Eng*. 2015;14(2):569-597. doi:10.1007/s10518-015-9819-x
5. Tubaldi E, Mitoulis S, Ahmadi H, Muhr A. A parametric study on the axial behaviour of elastomeric isolators in multi-span bridges subjected to horizontal seismic excitations. *Bull Earthquake Eng*. 2016;14(4):1285-1310. doi:10.1007/s10518-016-9876-9
6. Zhou Z, Wong J, Mahin S. Potentiality of using vertical and three-dimensional isolation systems in nuclear structures. *Nucl Eng Technol*. 2016;48(5):1237-1251.
7. Derham C, Kelly J, Thomas AG. Nonlinear natural rubber bearings for seismic isolation. *Nucl Eng Des*. 1985;84(3):417-428. doi:10.1016/0029-5493(85)90258-4
8. Kelly JM. Analysis of fiber-reinforced elastomeric isolators. *J Earthq Eng*. 1999;2(1):19-34.
9. Toopchi-Nezhad H, Tait MJ, Drysdale RG. Shake table study on an ordinary low-rise building seismically isolated with SU-FREIs (stable unbonded-fiber reinforced elastomeric isolators). *Earthq Eng Struct Dyn*. 2009;38(11):1335-1357.
10. Losanno D, Calabrese A, Madera-Sierra IE, et al. Recycled versus natural-rubber fiber-reinforced bearings for base isolation: review of the experimental findings. *J Earthquake Eng*. 2022;26(4):1921-1940. doi:10.1080/13632469.2020.1748764
11. Kelly J. *Base Isolation in Japan*. Earthquake Engineering Research Center, College of Engineering, University of California; 1988.
12. Aiken I, Kelly J, Tajirian F. *Mechanics Of Low Shape Factor Elastomeric Seismic Isolation Bearings*. Earthquake Engineering Research Center, College of Engineering, University of California, Berkeley. Report No. UCB/EERC-89/13; 1989.
13. Okamura S, Kamishima Y, Negishi K, Sakamoto Y, Kitamura S, Kotake S. Seismic isolation design for JSFR. *J Nucl Sci Technol*. 2011;48(4):688-692. doi:10.1080/18811248.2011.9711750
14. Cilento F, Vitale R, Spizzuoco M, Serino G, Muhr A, Analysis of the experimental behaviour of low shape factor isolation rubber bearings by shaking table investigation. In: XVII Convegno Anidis. 2017:21-30.
15. Yabana S, Matsuda A, Mechanical properties of laminated rubber bearings for three-dimensional seismic isolation. In: Proceedings of the 12th WCEE, 2000, New Zealand.
16. Warn G, Vu B. Exploring the low shape factor concept to achieve three dimensional seismic isolation. *Recent Innovations And Application Of Passive Seismic Control*. American Society of Civil Engineers; 2012:1-11. https://ascelibrary.org/doi/10.1061/9780784412374.001
17. Kelly J, Lee JJ. Vertical flexibility in isolation systems. *J Civ Eng Res*. 2018;4(1). doi:10.19080/cerj.2018.04.555629
18. Vemuru V, Nagarajaiah S, Masroor A, Mosqueda G. Dynamic lateral stability of elastomeric seismic 2 isolation bearings. *J Struct Eng*. 2014. doi:10.1061/(ASCE)ST.1943-541X.0000955. American Society of Civil Engineers: A4014014.
19. Vemuru VSM, Nagarajaiah S, Mosqueda G. Coupled horizontal–vertical stability of bearings under dynamic loading. *Earthquake Eng Struct Dyn*. 2016;45:913-934. 10.1002/eqe.2691
20. Ohsaki M, Miyamura T, Kohiyama M, Yamashita T, Yamamoto M, Nakamura N. Finite-element analysis of laminated rubber bearing of building frame under seismic excitation. *Earthquake Eng Struct Dyn*. 2015;44:1881-1898. doi:10.1002/eqe.2570
21. Kalfas K, Mitoulis S, Katakalos K. Numerical study on the response of steel-laminated elastomeric bearings subjected to variable axial loads and development of local tensile stresses. *Eng Struct*. 2017;134:346-357. doi:10.1016/j.engstruct.2016.12.015
22. Orfeo A, Tubaldi E, Muhr A, Losanno D. Mechanical behaviour of rubber bearings with low shape factor. *Eng Struct*. 2022.
23. Tubaldi E, Mitoulis S, Ahmadi H, Muhr A. parametric study on the axial behaviour of elastomeric isolators in multi-span bridges subjected to horizontal seismic excitations. *Bull Earthquake Eng*. 2016;14(4):1285-1310. doi:10.1007/s10518-016-9876-9
24. Kikuchi M, Aiken I. An analytical hysteresis model for elastomeric seismic isolation bearings. *Earthq Eng Struct Dyn*. 1997;26(2):215-231. doi:10.1002/(sici)1096-9845(199702)26:2⟨215::aid-eqe640⟩3.0.co;2-9
25. Kumar M, Whittaker A, Constantinou M. An advanced numerical model of elastomeric seismic isolation bearings. *Earthq Eng Struct Dyn*. 2014;43(13):1955-1974. doi:10.1002/eqe.2431
26. Nagarajaiah S, Ferrell K. Stability of elastomeric seismic isolation bearings. *J Struct Eng (N Y)*. 1999;125(9):946-954.
27. Grant D, Fenves G, Whittaker A. Bidirectional modelling of high-damping rubber bearings. *J Earthquake Eng*. 2004;8(sup001):161-185. doi:10.1080/13632460409350524

28. Kumar M, Whittaker A. Cross-platform implementation, verification and validation of advanced mathematical models of elastomeric seismic isolation bearings. *Eng Struct.* 2018;175:926-943.

29. Cardone D, Flora A, Gesualdi G. Inelastic response of RC frame buildings with seismic isolation. *Earthq Eng Struct Dyn.* 2012;42(6):871-889. doi:10.1002/eqe.2250

30. Tubaldi E, Ragni L, Dall'Asta A, Ahmadi H, Muhr A. Stress softening behaviour of HDNR bearings: modelling and influence on the seismic response of isolated structures. *Earthq Eng Struct Dyn.* 2017;46(12):2033-2054. doi:10.1002/eqe.2897

31. Tubaldi E, Mitoulis SA, Ahmadi H. Comparison of different models for high damping rubber bearings in seismically isolated bridges. *Soil Dyn Earthquake Eng.* 2018;104:329-345.

32. Ragni L, Cardone D, Conte N, et al. Modelling and seismic response analysis of Italian code-conforming base-isolated buildings. *J Earthquake Eng.* 2018;22:198-230.

33. Koh CG, Kelly J. A simple mechanical model for elastomeric bearings used in base isolation. *Int J Mech Sci.* 1988;30(12):933-943.

34. Koh CG, Kelly J. Modeling of seismic isolation bearings including shear deformation and stability effects. ASME. *Appl Mech Rev.* 1989;42(11S):S113-S120. doi:10.1115/1.3152379

35. Schapery RA. Elastomeric bearing sizing analysis Part 1: spherical bearing. *Int J Solids Struct.* 2018;152–153:118-139.

36. Schapery RA. Elastomeric bearing sizing analysis Part 2: flat and cylindrical bearings. *Int J Solids Struct.* 2018;152–153:140-150.

37. Schapery RA. Shim analysis for spherical elastomeric bearings. *Int J Solids Struct.* 2018;144–145:276-288.

38. Stanton JF, Scroggins G, Taylor AW, Roeder CW. Stability of laminated elastomeric bearings. *J Eng Mech.* 1990;116(6):1351-1371.

39. Muhr AH, Lateral stiffness of rubber mounts under finite axial deformation. In: Constitutive Model for Rubber X - Proceeding of the European Conference on Constitutive Model for Rubber, ECCMR X. 2017;153-158.

40. Gent AN. Elastic stability of rubber compression springs. *J Mech Eng Sci.* 1964;6(4):318-326.

41. Cilento F, Vitale R, Spizzuoco M, Serino G, Muhr AH, Dynamic Behaviour in Compression and Shear of Low Shape Factor Rubber Blocks, in [Atti del XVII Convegno ANIDIS L'ingegneria Sismica in Italia : Pistoia, 17–21. 2017. - (Studi in tema di internet ecosystem)][Pisa : Pisa University Press, 2017.] - Permalink: http://digital.casalini.it/4215750

42. Ragni L, Tubaldi E, Dall'Asta A, Ahmadi H, Muhr A. Biaxial shear behaviour of HDNR with Mullins effect and deformation-induced anisotropy. *Eng Struct.* 2018;154:78-92.

43. Chopra AK. *Dynamics of Structures: Theory and Applications to Earthquake Engineering.* Prentice Hall; 2012.

44. Cuomo G. Design, Development and Experimental Validation of Multilayer Modular Laminated Natural Rubber Isolators *Naples.* University of Naples Federico II; 2014.

45. Gough J, Muhr AH, Initiation of failure of rubber close to bondlines. *Proc. International Rubber Conference.* 2005, Maastricht. IOM Communications Ltd, London, 165-174.

46. Aiken ID, Kelly JM, Clark PW, Tamura K, Kikuchi M, Itoh T, Experimental studies of mechanical characteristics of three types of seismic isolation bearings. In: 10th World Conference on Earthquake Engineering; 1992.

47. Nagarajaiah S, Ferrell K. Stability of elastomeric seismic isolation bearings. *J Struct Eng (N Y).* 1999;125(9):946-954.

48. Thomas AG. The design of laminated bearings I. Proceeding conf. *NR Earthq Prot Build.* 1982:229-246.

49. Raithel A, Serino G. *Stabilità e Comportamento Post-Critico degli Isolatore Elastomerici Armati, 6° Convegno Nazionale L'Ingegneria Sismica in Italia, 13-15 Ottobre*; 1993.

50. INTERNATIONAL ATOMIC ENERGY AGENCY, *Seismic Isolation Systems for Nuclear Installations, IAEA-TECDOC-1905*, IAEA; 2020.

51. Goodchild IR, Muhr AH, Thomas AG. The lateral stiffness and damping of a stretched rubber beam. *Plast Rubber Compos.* 2018;47(4):176-186.

52. Buckle I, Nagarajaiah S, Ferrell K. Stability of elastomeric isolation bearings: experimental study. *J Struct Eng (N Y).* 2002;128(1):3-11.

53. Haringx JA. On highly compressible helical springs and rubber rods, and their application for vibration-free mountings. *Part I Philips Res Rep.* 1948;3(6):401.

54. Kosten CW. *Over de elastische eigenschappen van gevulcaniseerde rub- ber. (On the elastic properties of vulcanized rubber).* Thesis presented to Delft University; 1942. In partial fulfillment of the requirements for the degree of Doctor of Philosophy (in Dutch.

55. Gent AN, Lindley PB. The compression of bonded rubber blocks. *Rubber Chem Technol.* 1959;173(1):111-122. doi:10.1243/PIME_PROC_1959_173_022_02

56. Gent AN, Meinecke EA. Compression, bending, and shear of bonded rubber blocks. *Polym Eng Sci.* 1970;10:48-53. doi:10.1002/pen.760100110

57. Roeder CW, Stanton JF, Design of laminated elastomeric bridge bearings. In: Bridge Engineering Conference, 3rd, 1991, Denver, Colorado, USA; 1991.

58. Muhr AH, Effect of thickness of reinforcing plates on rubber-steel laminated bearings. In: 6th World conference on joints and bearings and seismic systems for concrete structures, Halifax, 2006;17-21

59. Kelly JM, Konstantinidis D. *Mechanics of rubber bearings for seismic and vibration isolation.* John Wiley & Sons; 2011.

60. Tubaldi E, Mitoulis SA, Ahmadi H. Comparison of different models for high damping rubber bearings in seismically isolated bridges. *Soil Dyn Earthq Eng.* 2018;104:329-345.

61. Crowder AP, Becker TC. Experimental investigation of elastomeric isolation bearings with flexible supporting columns. *J Struct Eng.* 2017;143(7):04017057. doi:10.1061/(ASCE)ST.1943-541X.0001784

62. Chang C. Modeling of laminated rubber bearings using an analytical stiffness matrix. *Int J Solids Struct.* 2002;39:6055-6078.

63. Warn GP, Whittaker AS, Constantinou MC. Vertical stiffness of elastomeric and lead-rubber seismic isolation bearings. *J Struct Eng*. 2007;133(9):1227-1236.

64. Losanno D, Spizzuoco M, Calabrese A. Bidirectional shaking-table tests of unbonded recycled-rubber fiber-reinforced bearings (RR-FRBs). *Struct Contr Health Monit*. 2019;26(9):e2386.

65. Losanno D, Madera Sierra IE, Spizzuoco M, Marulanda J, Thomson P. Experimental performance of unbonded polyester and carbon fiber reinforced elastomeric isolators under bidirectional seismic excitation. *Eng Struct*. 2020;209(110003):110003.

66. Calabrese A, Spizzuoco M, Serino G, Della Corte G, Maddaloni G. Shaking table investigation of a novel, low-cost, base isolation technology using recycled rubber. *Struct Contr Health Monit*. 2015;22(1):107-122.

67. Van Overschee P, De Moor BL. *Subspace Identification for Linear Systems: Theory — Implementation — Applications*. 1996th ed. Springer; 2012. Accessed March 15, 2021. https://www.springer.com/gp/book/9781461380610

68. Magliulo G, Petrone C, Capozzi V, Maddaloni G, Lopez P, Manfredi G. Seismic performance evaluation of plasterboard partitions via shake table tests. *Bull Earthq Eng*. 2013;12(4):1657-1677. doi:10.1007/s10518-013-9567-8

69. Pastor M, Binda M, Harčarik T. Modal assurance criterion. *Proc Eng*. 2012;48:543-548. doi:10.1016/j.proeng.2012.09.551. ISSN 1877–7058.

70. MATLAB. *version 7.10.0 (R2021b)*. The MathWorks Inc; 2021

71. Wang T, Wang F, Three-dimensional base-isolation system using thick rubber bearings. Proc. SPIE. 2012;8341, Active and Passive Smart Structures and Integrated Systems 2012, 83412K; doi:10.1117/12.916965

72. Losanno D, De Domenico D, Madera-Sierra IE. Experimental testing of full-scale fiber reinforced elastomeric isolators (FREIs) in unbounded configuration. *Eng Struct*. 2022;260:114234. doi:10.1016/j.engstruct.2022.114234